Journal of Alloys and Compounds 649 (2015) 625–629

Contents lists available at ScienceDirect

Journal of Alloys and Compounds

journal homepage: http://www.elsevier.com/locate/jalcom

Recovering near-band-edge ultraviolet responses in a wide-bandgap oxide with dipole-forbidden bandgap transition

Rui Deng [a, b], Yong-Feng Li [b, c, **], Bin Yao [b, c, *], Zhan-Hui Ding [b], Xuan Fang [d], Jie-Ming Qin [a], Zhi-Peng Wei [d], Qing-Cheng Liang [a], Lei Liu [e]

[a] School of Materials Science and Engineering, Changchun University of Science and Technology, Changchun 130022, China
[b] State Key Lab of Superhard Materials and College of Physics, Jilin University, Changchun 130023, China
[c] Key Laboratory of Physics and Technology for Advanced Batteries (Ministry of Education), College of Physics, Jilin University, Changchun 130012, China
[d] State Key Laboratory on High-Power Semiconductor Lasers, Changchun University of Science and Technology, 7186 Wei-Xing Road, Changchun 130022, China
[e] State Key Laboratory of Luminescence and Applications, Changchun Institute of Optics, Fine Mechanics and Physics, Chinese Academy of Sciences, No.3888 Dongnanhu Road, Changchun 130033, China

ARTICLE INFO

Article history:
Received 30 April 2015
Received in revised form
16 July 2015
Accepted 20 July 2015
Available online 22 July 2015

Keywords:
SnO_2 nanobelt
Ultraviolet photodiode
First-principles calculation
Photoluminescence

ABSTRACT

High-density SnO_2 nanobelts were synthesized on p-Si substrate to form a SnO_2 nanobelts/p-Si heterojunction photodiode. The photodiode shows a rectification characteristic in current–voltage measurements and exhibits an ultraviolet peak responsivity with an ultraviolet–visible rejection ratio (R395 nm/R550 nm) of two orders of magnitude. The peak responsivity is located at around 395 nm (3.14 eV), much smaller than optical absorption edge of bulk SnO_2 (~344 nm, 3.6 eV). A strong ultraviolet peak from SnO_2 nanobelts at ~400 nm was observed in the photoluminescence spectrum, indicating that the dipole-forbidden rule of bulk SnO_2 is broken for the nanostructural counterparts. First-principles calculations suggest that surface state in nanostructure plays a key role in breaking dipole forbidden rule and realizing ultraviolet peak responsivity.

1. Introduction

Ultraviolet (UV) photodetectors have attracted much attention due to their wide applications in optoelectronic fields [1–6]. Comparing to traditional Si-based UV detector, a kind of UV detectors based wide-bandgap semiconductor, such as SiC, GaN and ZnO etc, demonstrates outstanding performance owing to their high thermal stability, high responsivity and high response speed [7–15]. Among numerous wide-bandgap semiconductors, SnO_2 should be an ideal material and applied as high-performance UV detector due to its appropriate optical bandgap of ~3.6 eV [16]. However, it is commonly believed that SnO_2 is not a suitable material applied to UV photodiode because its dipole-forbidden nature of its band-edge quantum states leading to the weak UV absorption at fundamental bandgap [17]. Recent research indicates that the dipole-forbidden rule of SnO_2 can be broken via nanoengineering and doping-engineering. For example, strong UV emission can be recovered in SnO_2 nanowires, quantum dots [16–20]. First-principles calculations predicted that a large number of dangling bonds at surface of nanostructural SnO_2 can break the dipole-forbidden rule and enhance UV absorption at fundamental bandgap. It is deduced that SnO_2 based on nanostructure is a suitable materials used to fabricate high-performance UV detector. Recently, Hsu et al. fabricated a SnO_2-nanowire UV detector via forming p-SnO_2:Ga/n-Ga_2O_3 core–shell nanowires [21]. However, the fabrication methods of SnO_2 core–shell nanowires is complicated and uncontrollable. By contrast, some nanostructures, such as nanobelts and nanowires, has an advantage of a simple method for preparation [22–25]. Hu et al. reported an UV photodetector based on individual SnO_2 nanowire [26]. Nevertheless, it is also a complicated process to manipulate individual nanowire to fabricate device. Therefore, it is significantly important to develop a facile route to fabricate UV detector based on SnO_2 nanostructures.

In this paper, we fabricated SnO_2 nanobelts (NBs) on p-type Si substrate to form a SnO_2 NBs/p-Si heterojunction UV detector. The

* Corresponding author. Key Laboratory of Physics and Technology for Advanced Batteries (Ministry of Education), College of Physics, Jilin University, Changchun 130012, China.
** Corresponding author. State Key Lab of Superhard Materials and College of Physics, Jilin University, Changchun 130023, China.
E-mail addresses: liyongfeng@jlu.edu.cn (Y.-F. Li), binyao@jlu.edu.cn (B. Yao).

http://dx.doi.org/10.1016/j.jallcom.2015.07.186
0925-8388/

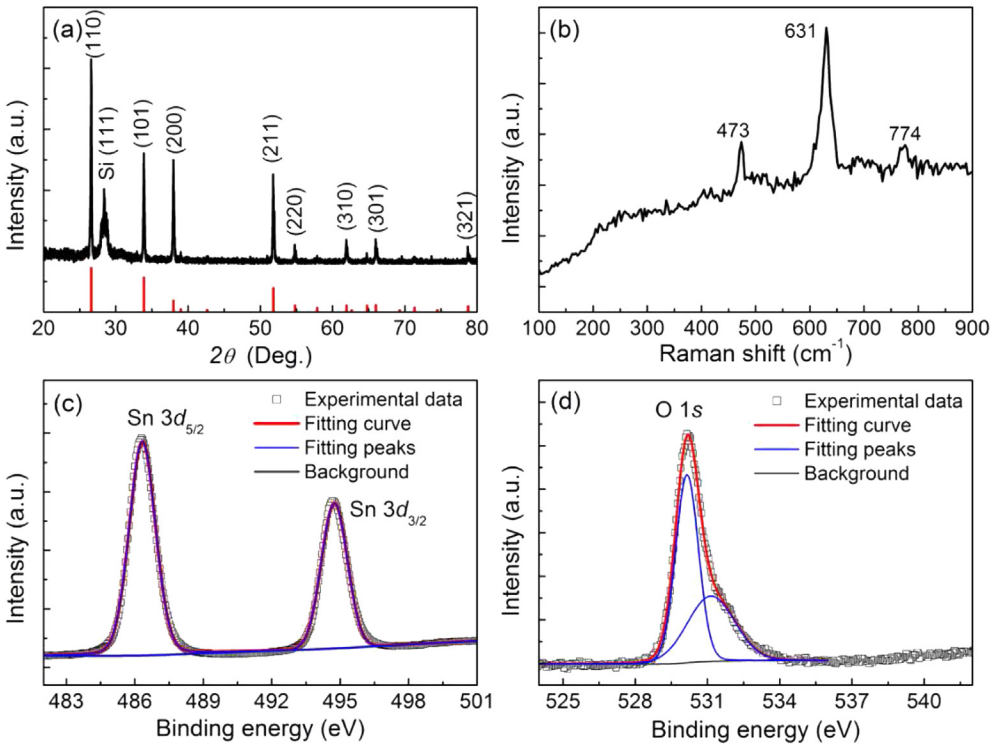

Fig. 1. (a) XRD pattern of the SnO_2 NBs synthesized on p-Si substrate. The reference powder diffraction data (PDF#880287) is also presented. (b) Raman spectrum of the SnO_2 NBs. (c–d) Sn 3*d* and O 1*s* XPS spectra of the SnO_2 NBs.

performance of the UV detector based on SnO_2 NBs was investigated in detail. A responsivity of ~10^{-4} A/W at fundamental bandgap of SnO_2 was obtained, in agreement with the recovered UV emission observed in the photoluminescence (PL) spectrum. The physical mechanism of breaking dipole-forbidden rule was also discussed through first-principles calculations.

2. Experimental and first-principles calculation detail

SnO_2 NBs were synthesized on p-type Si substrate using chemical vapor transport method. The synthesis process was carried out in a quartz tube located at a horizontal tube furnace. A mixture of SnO_2 and graphite powders (at a weight ratio of 2:1) acts as the precursor. A constant 100 cm^3/min flow of 95.5% Ar/0.5% O_2 was introduced to the tube during the growth process. The pressure in the tube furnace was fixed at 10 mbar, and the furnace temperature was increased to 950 °C and held there for 15 min. As finishing the growth process, the furnace was cooled to room temperature and then the products were taken out from the furnace. An Au finger electrode was deposited on SnO_2 NBs/p-Si sample using a shadow mask and an Al back electrode was deposited on another side of Si substrate using thermal evaporation method to obtain a prototypical SnO_2-based photodiode.

For structural characterizations, X-ray diffraction (XRD) was carried out using a powder diffractometer with Cu Kα radiation. Raman and PL measurements were performed using a He–Cd laser with a 325-nm line as the excitation source. The optical dddabsorption spectra of the SnO_2 films were recorded by UV–vis–near infrared spectrophotometer. Surface morphologies of the SnO_2 NBs were characterized using a field-emission scanning electron microscope (SEM, Hitachi S-4800, Japan). A high-resolution transmission electron microscope (TEM, FEI Tecnai G2 20, USA) was used to examine the nanobelt size and crystalline structure in the SnO_2 NBs. XPS was performed by an ESCALAB 250 XPS instrument with Al Kα ($h\nu = 1486.6$ eV) X-ray radiation source, which can precisely calibrate work function and Fermi energy level. All XPS spectra were calibrated by the C 1s peak (284.6 eV). The current–voltage (I–V) characteristics of the SnO_2 NBs/p-Si heterojunction photodiode were measured using a Keithley 4200 semiconductor characterization system.

First-principles calculations were performed within the framework of density functional theory (DFT). The exchange-correlation energy was treated within the generalized gradient approximation (GGA) [27] using the functional of Perdew, Burke, and Ernzerhof (PBE) [28]. The structural relaxations used the projector augmented wave (PAW) method as implanted in the Vienna ab initio simulation package (VASP) [29]. The hybrid functional as proposed by Heyd, Scuseria, and Ernzerhof (HSE06) was employed to calculated electronic structure and optical properties [30]. For the Sn atoms, d states were treated as valence states. To simulate large ratio of surface to volume for NBs, we truncated the rutile SnO_2 along the (100) and (110) surfaces and investigated their electronic structures and optical properties. The cutoff energy for the plane-wave basis set is 400 eV.

3. Results and discussion

Fig. 1a shows a typical XRD pattern of the synthesized SnO_2 NBs. To clearly show the origin of these diffraction peaks, the reference powder diffraction data (PDF#880287) is also presented. All diffraction peaks can be indexed to the rutile phase SnO_2 besides Si (111), and no other phases are observed, indicating that these SnO_2 NBs have a single phase. To further investigate the crystalline structure of SnO_2 NBs, we also performed Raman spectroscopy measurements, as shown Fig. 1b. Three obvious Raman peaks were observed at room temperature. The three peaks located at 473, 631 and 774 cm^{-1} are ascribed to E_g, A_{1g} and B_{1g} mode of SnO_2, respectively, indicating that SnO_2

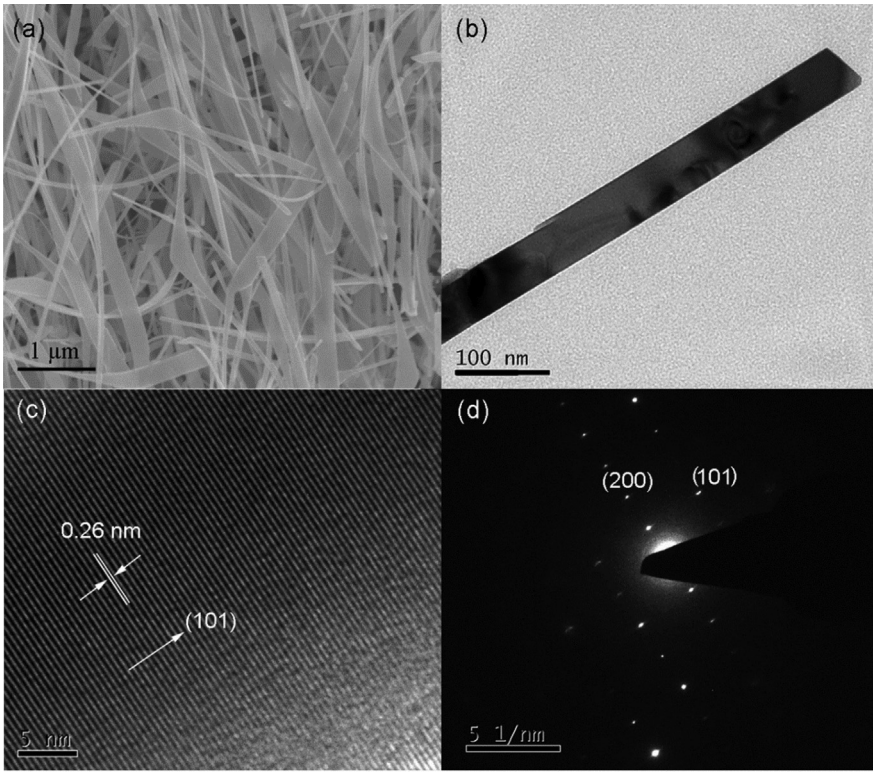

Fig. 2. (a) A typical FESEM image of the SnO_2 NBs synthesized on p-Si substrate. (b–c) Low- and high-resolution TEM images of an individual nanobelt. (d) The corresponding SAED pattern of the nanobelt.

NBs are pure phase and reconciles with XRD results. It should be noted that the wavenumber of the A_{1g} mode is lower than the bulk SnO_2 value of 638 cm^{-1}. This is agreed with the previous reports that the A_{1g} mode is sensitive to the size of SnO_2 and shifts to lower wavenumbers with decreasing SnO_2 sizes [31]. Fig. 1c and d show the Sn 3d and O 1s XPS spectra of the SnO_2 NBs. For the O 1s XPS spectrum, the strong peak at low binding energy side and weak shoulder at high energy side are attributed

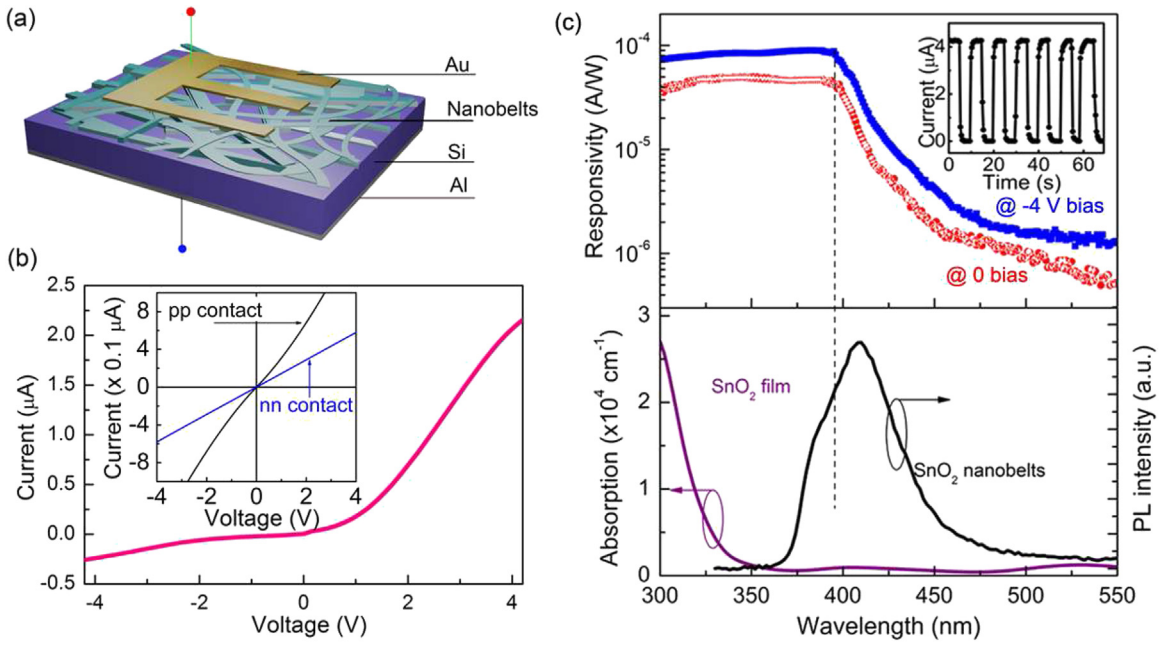

Fig. 3. (a) Schematic diagram of the SnO_2 NBs/p-Si heterojunction. (b) I–V curve of the SnO_2 NBs/p-Si heterojunction. The inset in (b) shows the I–V characteristics with Ohmic contacts between two gold contacts on the SnO_2 NBs as well as between two Al electrodes on the p-Si substrate. (c) Top panel: Room temperature spectral responses of the SnO_2 NBs/p-Si heterojunction with the applied voltage 0 and −4 V. The inset shows the time-dependent response of the photodiode measured under air conditions at zero bias as 390 nm light irradiating the device. Bottom panel: PL spectrum of SnO_2 NBs and optical absorption spectrum of a crystalline SnO_2 film for comparison.

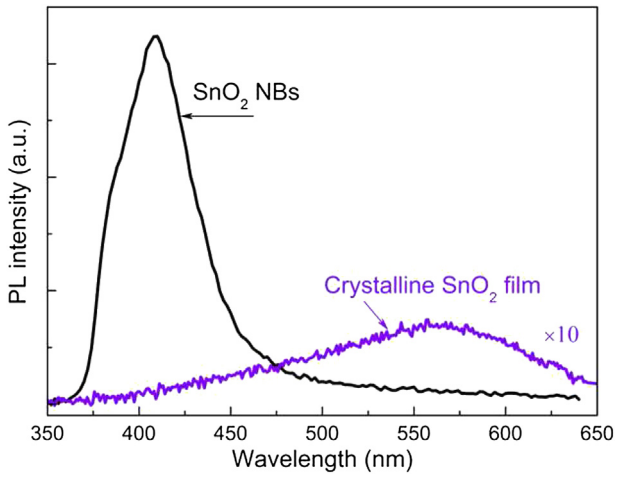

Fig. 4. Room temperature PL spectra of the SnO_2 nanobelts and crystalline SnO_2 film.

to the oxygen in the SnO_2 lattice and the adsorbed oxygen [32,33].

Fig. 2a shows a typical SEM image of the synthesized SnO_2 NBs. The sample is composed of large quantities of dense flattening NBs. The lengths and widths of these NBs are several tens of micrometers and several hundred nanometers, respectively. Fig. 2b shows a typical TEM image of an individual SnO_2 nanobelt. Fig. 2c shows a high-resolution TEM image of the enlarged region from the individual SnO_2 nanobelt. The lattice spacing of 0.26 nm reconciles with the (101) planes of rutile SnO_2. Fig. 2d shows the corresponding selected area electron diffraction (SEAD) pattern. The diffraction spots indicating that the SnO_2 nanobelt is single crystalline with the rutile SnO_2 structure.

To investigate the performance of SnO_2 NBs/p-Si heterojunction, the Au finger electrode and Al back electrode were deposited on NBs and Si sides using thermal evaporation method, respectively, to form a prototypical SnO_2 NBs/p-Si heterojunction photodiode. The structural schematic of the photodiode is shown in Fig. 3a. Fig. 3b shows the current–voltage (I–V) characteristics of the SnO_2 NBs/p-Si heterojunction photodiodes. The I–V curve shows a good rectification characteristic. The inset of Fig. 3b shows the ohmic contacts between two separated gold contacts on the SnO_2 NBs and between two Al back contacts on the p-Si substrate. The spectral responses of the SnO_2 NBs/p-Si photodiode at zero bias and the reverse bias of 4 V are shown in the top panel of Fig. 3c. A wide response range from 300 to 450 nm is observed and the response peak is located at ~395 nm (3.14 eV). The peak responsivity of the photodiode is determined to be 3×10^{-5} and 1×10^{-4} A/W at 395 nm (3.14 eV) at zero and the reverse bias of 4 V, respectively. Hsu et al. reported a responsivity of ~10^{-3} A/W (@395 nm) of SnO_2 photodetector using a complex Ga_2O_3/SnO_2:Ga core–shell nanowires structure [21]. The UV to visible rejection ratio (R395 nm/R550 nm) of two orders of magnitude was obtained at a reverse bias of 4 V. The inset in Fig. 3c shows the time-dependent photoresponse of the photodiode at air conditions as a periodical turning on and off 390 nm light irradiates on the device. The photocurrent increases to 4.3 μA and decreases to initial value, respectively, as the light was periodically turned on and off, suggesting the excellent reproducible characteristics.

To investigate the origin of response peak, PL spectrum of SnO_2 NBs were carried out at temperature, as shown in the bottom panel of Fig. 3c. There is a peak and a shoulder in the PL spectrum of the SnO_2 NBs. The PL peak and shoulder are located at 420 nm (2.95 eV) and 390 nm (3.18 eV), respectively. To illustrate the optical band edge of crystalline SnO_2, we performed the UV–visible optical absorption measurement for a crystalline SnO_2 film grown on quartz substrates, as shown in the bottom panel of Fig. 3c. The optical bandgap of crystalline SnO_2 film is at ~3.65 eV (340 nm), which is consistent with the previous reports on the value of bulk SnO_2. Both the PL peak and shoulder of SnO_2 NBs are much smaller than the optical bandgap of bulk SnO_2, indicating that the band-edge dipole-forbidden rule of bulk SnO_2 is broken by NBs and UV emission is recovered in SnO_2 NBs. The response peak at ~395 nm is very close to the PL shoulder and therefore it is derived from breaking dipole-forbidden rule via forming nanostructure. To further demonstrate how the SnO_2 NBs break dipole-forbidden rule of bulk SnO_2, we compared the PL spectra of SnO_2 NBs with the crystalline SnO_2 film, as shown in Fig. 4. For the crystalline SnO_2 film, only a weak visible emission band is observed and no UV emission is observed. However, strong UV near-band-edge (NBE) emission is observed, indicating that the dipole-forbidden rule is broken.

In order to elucidate the physical mechanism of nanostruture breaking dipole-forbidden rule, we performed first-principles calculations based on hybrid functional method. It is known that nanostructure has much larger ratio of surface to volume than bulk. To simulate the surface of SnO_2, we constructed a (100) and (110) plane orientated SnO_2 surfaces with a vacuum layer. We calculated the optical absorption spectra of bulk, (100) and (110) plane orientated SnO_2 surfaces, as shown in Fig. 5a. The calculated optical bandgap of bulk SnO_2 is determined to be 3.7 eV, in good accordance with the experimental value. The calculated fundamental bandgap is 3.2 eV for bulk SnO_2. For the (100) surface of SnO_2, the optical bandgap is has a slight redshift with respect to bulk SnO_2 and still larger than the fundamental bandgap of bulk SnO_2, indicating that the (100) surface is unable to break the dipole-forbidden rule. Nevertheless, a strong and broad absorption centered at

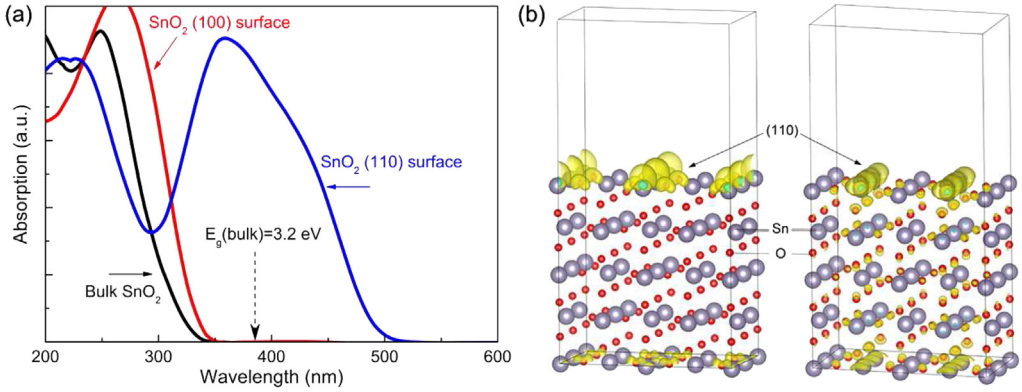

Fig. 5. First-principles calculated (a) absorption spectra of the bulk SnO_2 and the SnO_2 with (100) and (110) plane orientation surfaces as well as (b) charge density plots of the (110) plane orientated SnO_2 surface at E_F (left) and E_F+3.2 eV (right).

~3.1 eV (400 nm), covering the fundamental bandgap of SnO_2, is obtained for the (110) surface of SnO_2, indicating the forbidden fundamental bandgap becomes allowed. Thus, it is well understood why the response peak of SnO_2 NBs/p-Si photodiode is much smaller than the optical bandgap of bulk SnO_2. Additionally, there is a wide absorption band from 300 to 500 nm for the (110) surface of SnO_2, supporting and explaining the wide response range in the spectral response of the SnO_2 NBs photodiode.

To well understand the electron transition corresponding to the fundamental bandgap, we calculated the charge density distribution of the (110) surface of SnO_2 at Fermi level (E_F) and E_F+3.2 eV, as shown in Fig. 5b. It is found that the charge densities at E_F and E_F+3.2 eV are manly distributed in the (100) surface region. This result suggests that the electron transition corresponding to light emission or absorption occurs in the surface region and also confirms the surface-associated local symmetry breaking are responsible for the interband transition.

4. Conclusions

In summary, we synthesized SnO_2 NBs on p-Si substrate to form a SnO_2 NBs/p-Si heterojunction photodiode. The performance of the photodiode was characterized. A UV peak responsivity with an UV–visible rejection ratio (R395 nm/R550 nm) of two orders of magnitude is observed at the bias of 0 and −4 V. First-principles calculations suggest that surface states are responsible for breaking dipole forbidden rule of SnO_2 and realizing UV peak responsivity.

Acknowledgments

This work was supported by the National Natural Science Foundation of China under Grant Nos. 10874178, 11074093, 61205038, 11464035, and 11274135, Natural Science Foundation of Jilin province under Grant No. 201115013, and 20140101052JC, and National Found for Fostering Talents of Basic Science under Grant No. J1103202, and Ph.D. Programs Foundation of Ministry of Education of China under Grant No. 20120061120011, and the Scientific and Technological Development Project of Jilin Province No. 20150311086YY. This work was supported by High Performance Computing Center of Jilin University, China.

References

[1] Y.F. Li, B. Yao, R. Deng, B.H. Li, J.Y. Zhang, Y.M. Zhao, D.Y. Jiang, Z.Z. Zhang, C.X. Shan, D.Z. Shen, X.W. Fan, Y.M. Lu, J. Phys. D Appl. Phys. 42 (2009) 105102.
[2] P.S. Shewale, N.K. Lee, S.H. Lee, K.Y. Kang, Y.S. Yu, J. Alloys Compd. 624 (2015) 251–257.
[3] M. Zhang, D. Li, J. Zhou, W. Chen, S. Ruan, J. Alloys Compd. 618 (2015) 233–235.
[4] C. Gao, X. Li, X. Zhu, L. Chen, Y. Wang, F. Teng, Z. Zhang, H. Duan, E. Xie, J. Alloys Compd. 616 (2014) 510–515.
[5] D. Zhang, X. Gu, F. Jing, F. Gao, J. Zhou, S. Ruan, J. Alloys Compd. 618 (2015) 551–554.
[6] K. Lv, M. Zhang, C. Liu, G. Liu, H. Li, S. Wen, Y. Chen, S. Ruan, J. Alloys Compd. 580 (2013) 614–617.
[7] H. Ohta, M. Kamiya, T. Kamiya, M. Hirano, H. Hosono, Thin Solid Films 445 (2003) 317–321.
[8] T.-H. Moon, M.-C. Jeong, W. Lee, J.-M. Myoung, Appl. Surf. Sci. 240 (2005) 280–285.
[9] M. Asif Khan, J.N. Kuznia, D.T. Olson, M. Blasingame, A.R. Bhattarai, Appl. Phys. Lett. 63 (1993) 2455–2456.
[10] M.A. Abbasi, Z.H. Ibupoto, A. Khan, O. Nur, M. Willander, Mater. Lett. 108 (2013) 149–152.
[11] L. Guo, H. Zhang, D. Zhao, B. Yao, B. Li, Z. Zhang, D. Shen, Mater. Lett. 65 (2011) 1495–1498.
[12] J. Kim, J.-H. Yun, S.-W. Jee, Y.C. Park, M. Ju, S. Han, Y. Kim, J.-H. Kim, W.A. Anderson, J.-H. Lee, J. Yi, Mater. Lett. 65 (2011) 786–789.
[13] G.Z. Xing, Y.H. Lu, Y.F. Tian, J.B. Yi, C.C. Lim, Y.F. Li, G.P. Li, D.D. Wang, B. Yao, J. Ding, Y.P. Feng, T. Wu, AIP Adv. 1 (2011) 022152.
[14] D. Wang, G. Xing, X. Wang, D. Yin, M. Zhou, Q. Guo, J. Yang, L. Yang, J. Cao, Y. Yan, Mater. Res. Bull. 46 (2011) 937–940.
[15] A. Echresh, C.O. Chey, M. Zargar Shoushtari, V. Khranovskyy, O. Nur, M. Willander, J. Alloys Compd. 632 (2015) 165–171.
[16] Y. Li, R. Deng, Y. Tian, B. Yao, T. Wu, Appl. Phys. Lett. 100 (2012) 172402.
[17] Y. Li, W. Yin, R. Deng, R. Chen, J. Chen, Q. Yan, B. Yao, H. Sun, S.-H. Wei, T. Wu, NPG Asia Mater. 4 (2012) e30.
[18] H. Zhou, R. Deng, Y.-F. Li, B. Yao, Z.-H. Ding, Q.-X. Wang, Y. Han, T. Wu, L. Liu, J. Phys. Chem. C 118 (2014) 6365–6371.
[19] R. Chen, G.Z. Xing, J. Gao, Z. Zhang, T. Wu, H.D. Sun, Appl. Phys. Lett. 95 (2009) 061908.
[20] S. Brovelli, N. Chiodini, R. Lorenzi, A. Lauria, M. Romagnoli, A. Paleari, Nat. Commun. 3 (2012) 690–693.
[21] C.-L. Hsu, Y.-C. Lu, Nanoscale 4 (2012) 5710–5717.
[22] F.K. Butt, C. Cao, W.S. Khan, M. Safdar, X. Fu, M. Tahir, F. Idrees, Z. Ali, G. Nabi, D. Yu, CrystEngComm 15 (2013) 2106–2112.
[23] F.K. Butt, C. Cao, W.S. Khan, Z. Ali, T. Mahmood, R. Ahmed, S. Hussain, G. Nabi, Mater. Chem. Phys. 136 (2012) 10–14.
[24] F.K. Butt, C. Cao, T. Mahmood, F. Idrees, M. Tahir, W.S. Khan, Z. Ali, M. Rizwan, M. Tanveer, S. Hussain, I. Aslam, D. Yu, Mater. Sci. Semicond. Process. 26 (2014) 388–394.
[25] S. Zaman, J. Xin, F.K. Butt, Mater. Lett. 119 (2014) 111–114.
[26] L. Hu, J. Yan, M. Liao, L. Wu, X. Fang, Small 7 (2011) 1012–1017.
[27] J.P. Perdew, K.A. Jackson, M.R. Pederson, D.J. Singh, C. Fiolhais, Phys. Rev. B 46 (1992) 6671–6687.
[28] J.P. Perdew, K. Burke, M. Ernzerhof, Phys. Rev. Lett. 77 (1996) 3865–3868.
[29] P.E. Blöchl, Phys. Rev. B 50 (1994) 17953–17979.
[30] J. Heyd, G.E. Scuseria, M. Ernzerhof, J. Chem. Phys. 118 (2003) 8207–8215.
[31] A. Dieguez, A. Romano-Rodrıguez, A. Vila, J.R. Morante, J. Appl. Phys. 90 (2001) 1550–1557.
[32] Y. Nagasawa, T. Choso, T. Karasuda, S. Shimomura, F. Ouyang, K. Tabata, Y. Yamaguchi, Surf. Sci. 433–435 (1999) 226–229.
[33] T. Kawabe, S. Shimomura, T. Karasuda, K. Tabata, E. Suzuki, Y. Yamaguchi, Surf. Sci. 448 (2000) 101–107.